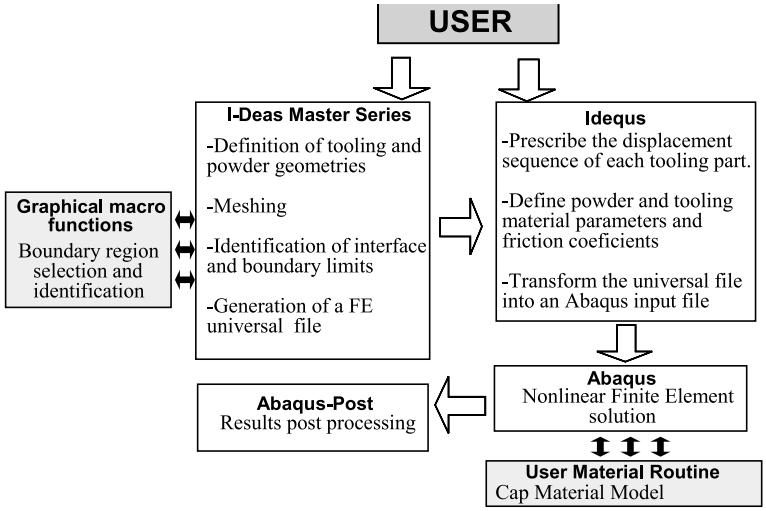

Fig. 3. Integrated simulation module.

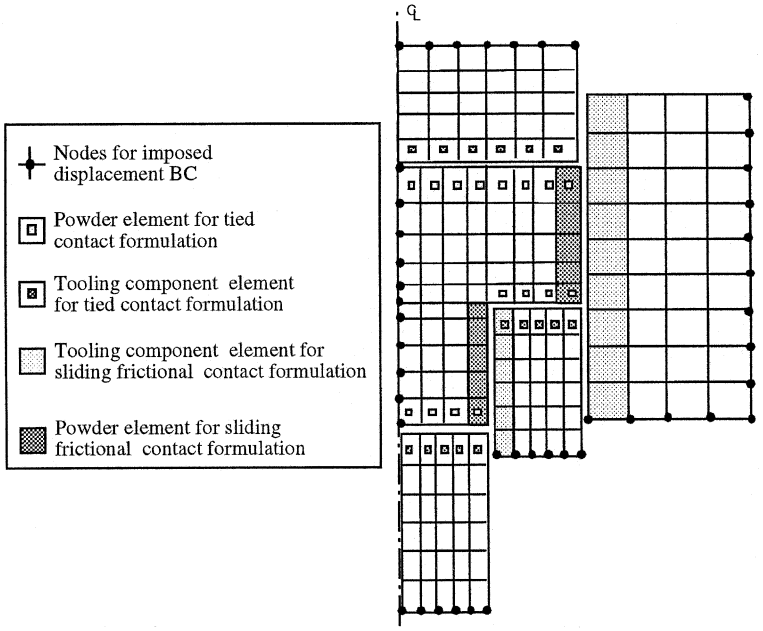

Fig. 4. Boundary regions identified by user developed macro-functions.

Large displacement contact with Coulomb friction was adopted for the interface regions between the powder cavity and tooling component sides. Moreover, since very small powder sliding occurs on punch faces, tied (sticking) contact was adopted for the these interface regions. The friction coefficient was assumed to be equal to 0.2 as in previous studies (Weber and Brown, 1989; Trasorras et al., 1989; Shima and Saleh, 1993) and its reliability was verified by comparing simulated results with experimental measurements as discussed in Section 6. Both contact conditions were modeled using the "master-slave" contact pair

formulation of ABAQUS (HKS, 1995b). This formulation requires the association of the master surface with the stiffer interacting body (tooling component) whereas the slave surface is associated with the second deformable body (powder cavity). IDEQUS automatically identifies, generates and pairs off contact surfaces using the element sets selected by the macro functions.

All the information is written to a universal FE file which is then completed with additional information and then translated into the ABAQUS format by way of the IDEQUS program. This tool also permits to:

- Define powder and tooling material parameters as well as friction coefficients.
- Prescribe the displacement sequence of each tooling component.
- Define the solution control parameters.

4.3. Processing and post-processing

ABAQUS is a FE solver capable of handling both geometric and material nonlinearities, as well as the frictional contact nonlinearities. One of its main advantages is the open facility it offers for the definition of user material models. In fact, the cap material model was implemented into ABAQUS via the UMAT facility that allows the user to define a constitutive model and implement its numerical integration algorithm as a Fortran subroutine (HKS, 1995b). Thus, UMAT is called by the main program at each element integration point within every equilibrium iteration of each load increment of the deformation process. The global FE problem was solved using the classical Newton–Raphson method with a line-search algorithm whereas the local material integration was handled by the closest point projection algorithm (Simo, 1992; Koopman et al., 1992).

Finally, the ABAQUS-Post software (HKS, 1995a) is used mainly for the visualization of the predicted density maps within the compacts. The stress distribution, as well as the deformed shape of the tooling components, could also be post-processed by the same software.

5. Industrial application

5.1. Scope

In this section, a typical compaction case study is presented in order to illustrate the industrial use and to assess the predictive capabilities of the simulation module. The studied part is a three level axisymmetric part, made from the previously characterized 316L stainless steel powder and produced on an industrial basis (Fig. 5). It is compacted in a 250 t hydraulic press using a rigid die and a set of two upper and three lower punches, all made from tool steel.

Since the studied part production started before the simulation module had become operational, the use of this module was not for predictive purposes but for:

- the validation of simulation results;
- and for the investigation of part cracking problems.

First, we start by the simulation of the part compaction as it is performed in the production press. Then, the obtained density distribution is to be validated by comparing it with a second distribution obtained by the developed experimental technique. Finally, in order to solve the part cracking problem, the module is used for investigating the effects of change in the compaction sequence on the density gradient in the compact.

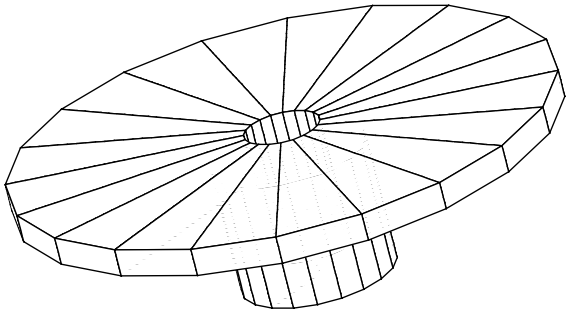

Fig. 5. Part geometry.

5.2. Data modeling

The data set required for the modeling activity includes the tooling geometry, the exact position of each tooling component at each compaction step including the filling and the pressing positions (Fig. 5) and the powder initial density in the cavity. Due to the densification resulting from the automatic press filling, this density is different from the apparent density given by the powder manufacturer. It should be calculated by dividing the final compact mass by the cavity volume. For this application, the initial relative density was 38% whereas apparent density given by the manufacturer was 33%.

As shown in Fig. 6 and Table 1, the first step of the compaction sequence is a powder transfer step, essential to press the lower (inner) level of the part. In order to avoid potential part cracking, any powder transfer operation should be completed prior to any effective compaction step. For this reason, we considered the post-transfer position as the initial modeling position. Thus, the effective compaction sequence consists of two steps.

5.3. Finite element mesh and boundary conditions

The powder initial geometry corresponds to the cavity shape after the powder transfer step whereas the tooling component geometry were simplified since no tooling stress analysis is involved in this study. Moreover, since lower punches 1 and 2 move in unison after powder transfer, they have been modeled as a single punch named "lower punch 1". ABAQUS CAX4 four node axisymmetric element (HKS, 1995b) was used to mesh the geometrical models of the tooling components as well as the powder cavity (Fig. 7).

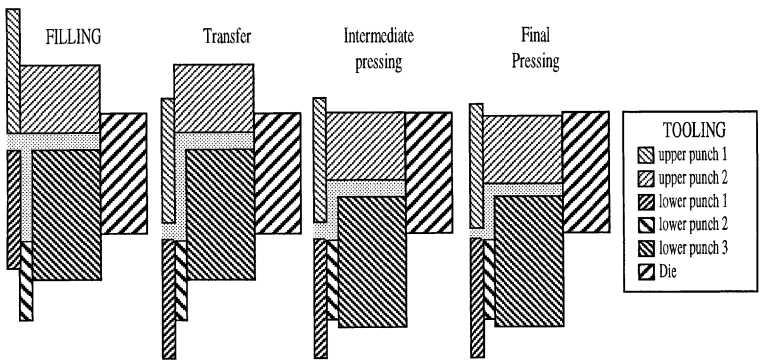

Fig. 6. Tooling and pressing sequence.

Table 1
Tooling positions

Tool	Positions			
	Filling	Transfer	Interm. pressing	Final
Upper punch 1	0	−26.6	−28.5	−28.5
Upper punch 2	0	0	−17.5	−17.5
Lower punch 1	−5	−31.6	−31.6	−31.1
Lower punch 2	−31.6	−31.6	−31.6	−31.1
Lower punch 3	−5.9	−5.9	−18.5	−18.5

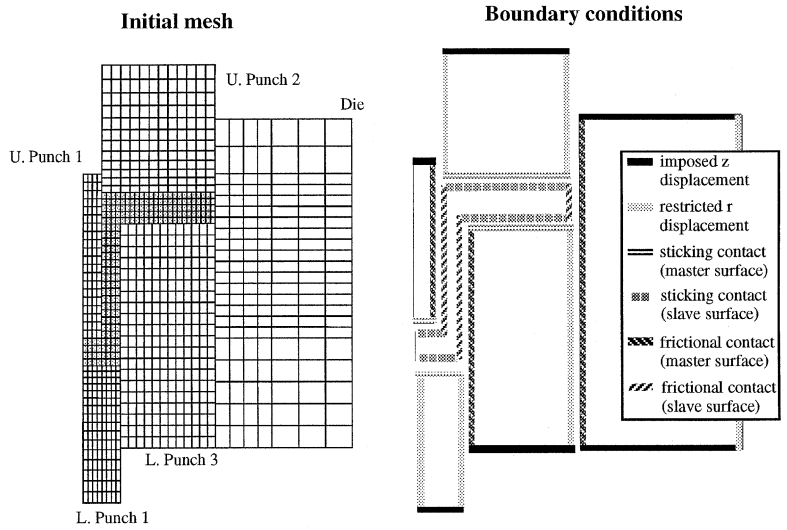

Fig. 7. Initial mesh and boundary conditions of the three-level part.

Ideas user's defined macro functions were implemented and used to identify specific interaction and boundary condition regions. IDEQUS was subsequently used to prescribe the boundary conditions for the analysis steps corresponding to the two sequence compaction steps. The friction coefficient between powder and tool sides was taken to be equal to 0.2 as in previous studies.

5.4. Results

The two-step FE problem was solved by ABAQUS with a relatively small number of increments for each one of the steps. In fact, only four increments were needed for each of the loading steps. In addition, the global Newton–Raphson solution scheme, as well as the local implementation scheme of the cap model, behaves very well. In fact, the number of global equilibrium iterations per increment ranged between 2 and 4. Besides, an average number of 7 local iterations were needed for the material integration algorithm at each global equilibrium iteration. The obtained density distribution is presented in Fig. 8.

In order to validate the simulation results, an experimental density map, presented (Fig. 9), was obtained by the method based on the correlation with Vickers hardness measures. [1] Globally, agreement between

[1] The inner level of the part was too weak to resist during the metallographic preparation procedure.

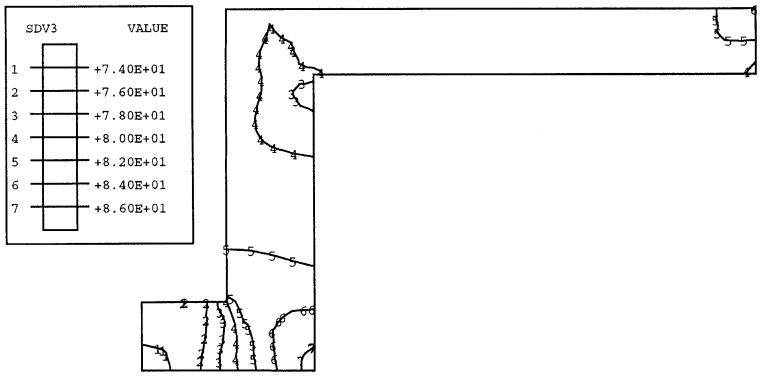

Fig. 8. Final shape and density distribution.

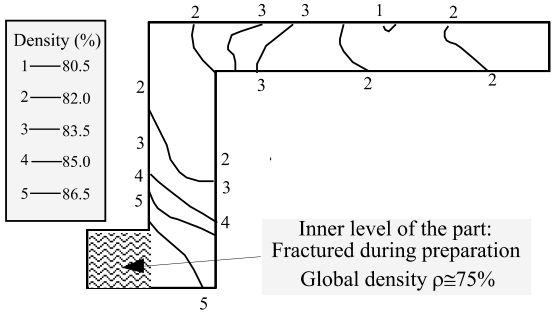

Fig. 9. Experimentally obtained density distribution.

simulated and experimental maps is within the density range of 1%, which is the accuracy of the experimental method (Guillot and Chtourou, 1996). This validation confirmed the high density gradient in the lower region of the part which constitutes a serious quality problem.

5.5. Improving part quality

As may be seen from the simulation and the experimental results, the compaction sequence used for this part led to a huge density gradient in the inner corner region. This gradient is very likely responsible of the noticed part cracking. Part quality could easily be improved by balancing the compaction sequence. This could simply be done by slightly increasing the filling height of the inner level together with an additional compaction of this region using upper punch 1. Furthermore, the compaction sequence could be simplified by using a single step instead of the two-step sequence. This solution was investigated by way of simulation featuring a new compaction sequence (Table 2) leading to the same final dimensions of the compact. Simulation results (Fig. 10) show that this new sequence effectively leads to a more homogeneous and stronger compact. Since results of this figure were intended to illustrate the use of the integrated module in compaction design and not to serve as model validation tests, no corresponding experimental results were obtained.

Table 2
Tooling positions according to the modified compaction sequence

Tool	Positions		
	Filling	Transfer	Final pressing
Upper punch 1	0	−25.6	−29.5
Upper punch 2	0	0	−17.5
Lower punch 1	−6	−31.6	−31.1
Lower punch 2	−31.6	−31.6	−31.1
Lower punch 3	−5.9	−5.9	−18.5

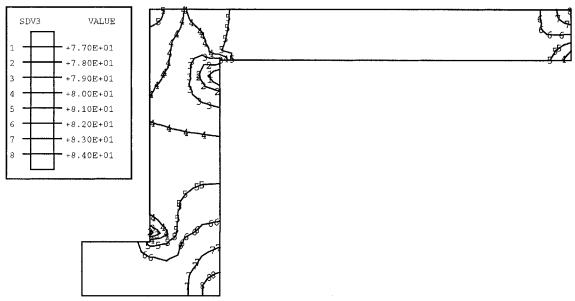

Fig. 10. Simulation results obtained using the modified sequence.

6. Conclusion

In the first (Chtourou et al., 2001) of a series of two papers on PM, the problem of experimental characterization of the material model for the 316L stainless steel powder was addressed together with its experimental validation procedure.

In this second part, computational aspects are addressed based on the FE simulation approach in an integrated simulation environment for industrial application. The problems of rigid die compaction of ductile metal powders involves material, geometric as well as boundary conditions (frictional contact) nonlinearities. While the last two nonlinearities were handled automatically by the ABAQUS FE solver, the first involve a material model unavailable in ABAQUS and hence the elastoplastic cap model had to be formulated and integrated into the software in order to be able to simulate the behavior of the metal powder medium. The closest point projection algorithm was used for the numerical integration of the multisurface plasticity model. Due to its flexibility and capacity to represent all the compaction stages, the cap material model was shown to yield very good results as far as the final density was the main concern and despite the fact that the model was not completely characterized. This is however expectable since the final density is mainly sensitive to the cap hardening parameters which seem to have been correctly identified. Since however no data was available about the shear failure mode the present model parameters cannot correctly simulate the ejection phase and associated residual stresses.

Finally, an integrated simulation environment has been developed and the simulation of the compaction of an industrial PM part has been performed successfully thus demonstrating the practical industrial applications of the computational approach. This application illustrates the modeling activity tasks and demonstrates the accuracy and the numerical efficiency of the implemented computational algorithms.

Further studies are still underway and concern the construction and calibration of a triaxial testing machine aimed at the gathering of the missing data (especially for the failure mode) or incomplete data on elastic behavior at low density levels. Also adjustment of material parameters through optimal parameters identification and inverse modeling process is considered. This will be applied in order to get rid of the current hypothesis of uniform deformation used in extracting material parameter values from the experimental measurements.

Acknowledgements

The authors would like to thank Mr. Sébastien Parent and Ms. Isabelle Jacob from Précitech Inc. for the experimental assistance as well as M. Christian Michaud, Mrs. Cathryn Macrander and M. André Hengartner for their help in software development. The authors would also like to acknowledge the support of the National Sciences and Engineering Research council of Canada (strategic grant no. 0167091 and grant no. CRD-186296).

Appendix A. Derivation of the algorithmically consistent tangent moduli of the cap model [2]

A.1. Case 1: Perfect plasticity

The first variation of the plastic strains is given by

$$\mathrm{d}\varepsilon^{\mathrm{p}}_{n+1} = \sum_i \left[\mathrm{d}(\Delta\lambda_i) \frac{\partial f_i}{\partial \sigma} + \Delta\lambda_i \frac{\partial^2 f_i}{\partial \sigma^2} : \mathrm{d}\sigma \right] \tag{A.1}$$

When combined with Eq. (21) the above relation gives

$$\mathrm{d}\sigma_{n+1} = \Xi : \left(\mathrm{d}\varepsilon_{n+1} - \sum_i \mathrm{d}(\Delta\lambda_i) \frac{\partial f_i}{\partial \sigma} \right) \tag{A.2}$$

where

$$\Xi^{-1} = C^{-1} + \sum_i \Delta\lambda_i \frac{\partial^2 f_i}{\partial \sigma^2} \tag{A.3}$$

This tensor could be inverted numerically or analytically using the Sherman–Morrison method (Hofstetter et al. 1993). This method is privileged since it is numerically cheaper. Furthermore, the plastic consistency parameters $\Delta\lambda_i$ are obtained by use of the normality condition of each of the active yield functions:

$$\mathrm{d}f_i = \frac{\partial f_i}{\partial \sigma} : \mathrm{d}\sigma = 0 \tag{A.4}$$

Using this relation and Eq. (A.3), one can define the following equation system in which $\Delta\lambda_i$ are the unknowns:

$$\sum_i \frac{\partial f_j}{\partial \sigma} : \Xi : \frac{\partial f_i}{\partial \sigma} \mathrm{d}(\Delta\lambda_i) = \frac{\partial f_j}{\partial \sigma} : \Xi : \mathrm{d}\varepsilon \tag{A.5}$$

[2] Subscripts i and j refer to the active yield surfaces.

This system can be more conveniently expressed as follows:

$$\sum_i g_{ji} \mathrm{d}(\Delta\lambda_i) = \frac{\partial f_j}{\partial \sigma} : \Xi : \mathrm{d}\varepsilon \tag{A.6}$$

where

$$g_{ji} = \frac{\partial f_j}{\partial \sigma} : \Xi : \frac{\partial f_i}{\partial \sigma} \tag{A.7}$$

which permits the determination of the plastic consistency parameters:

$$\mathrm{d}(\Delta\lambda_i) = \sum_j g_{ij}^{-1} \left(\frac{\partial f_j}{\partial \sigma} : \Xi : \mathrm{d}\varepsilon \right) \tag{A.8}$$

Finally, the integration of this last relation into Eq. (A.3) we can express the elastoplastic tangent moduli as

$$\frac{\mathrm{d}\sigma_{n+1}}{\mathrm{d}\varepsilon_{n+1}} = \Xi - \sum_i \sum_j g_{ij}^{-1} \left(\Xi : \frac{\partial f_i}{\partial \sigma} \otimes \Xi : \frac{\partial f_j}{\partial \sigma} \right) \tag{A.9}$$

A.2. Case 2: Hardening plasticity (cap mode)

Since the yield function of the cap mode involves the hardening parameter k, the first variation of plastic strains is given by

$$\mathrm{d}\varepsilon^{\mathrm{p}} = \mathrm{d}(\Delta\lambda_3) \frac{\partial f_3}{\partial \sigma} + \Delta\lambda_3 \left(\frac{\partial^2 f_3}{\partial \sigma^2} : \mathrm{d}\sigma + \frac{\partial^2 f_3}{\partial \sigma \, \partial k} : \mathrm{d}k \right) \tag{A.10}$$

Incorporating Eq. (A.10) into Eq. (21), and using the same tensor Ξ defined by Eq. (A.3), one can obtain:

$$\mathrm{d}\sigma = \Xi : \mathrm{d}\varepsilon - \Xi : \frac{\partial f_3}{\partial \sigma} \mathrm{d}(\Delta\lambda_3) - \Delta\lambda_3 \Xi : \frac{\partial^2 f_3}{\partial \sigma \, \partial k} \mathrm{d}k \tag{A.11}$$

In addition, the derivation of cap yield function relatively to its two independent variables gives:

$$\mathrm{d}f_3 = \frac{\partial f_3}{\partial \sigma} : \mathrm{d}\sigma + \frac{\partial f_3}{\partial k} : \mathrm{d}k = 0 \tag{A.12}$$

Furthermore, in order to completely define the problem we should introduce the incremental form of the hardening law (Eq. (A.13)) as well as its derivative (Eq. (A.14)):

$$\frac{1}{3} \Delta I^{\mathrm{p}}(k) - \Delta\lambda_3 \frac{\partial f_3}{\partial J} = 0 \tag{A.13}$$

$$\frac{1}{3} \frac{\mathrm{d}(\Delta I^{\mathrm{p}}(k))}{\mathrm{d}k} \mathrm{d}k - \mathrm{d}(\Delta\lambda_3) \frac{\partial f_3}{\partial J} - \Delta\lambda_3 \times \left(\frac{\partial^2 f_3}{\partial J \, \partial \sigma} : \mathrm{d}\sigma + \frac{\partial^2 f_3}{\partial J \, \partial k} : \mathrm{d}k \right) = 0 \tag{A.14}$$

Finally, this last relation combined with Eq. (A.12) in which Eq. (A.11) is inserted, gives the expression of tangent moduli:

$$\frac{\mathrm{d}\sigma_{n+1}}{\mathrm{d}\varepsilon_{n+1}} = \Xi - \sum_i \sum_j a_{ij}^{-1} \left(\Xi : \frac{\partial f_3}{\partial \sigma} \otimes \Xi : \frac{\partial^2 f_3}{\partial \sigma \, \partial k} \right) \tag{A.15}$$

where subscripts i and j do not refer any more to active yield surfaces but simply takes the values 1 and 2 and where coefficients a_{ij}^{-1} are the components of the inverse of matrix **a** defined by:

$$a_{11} = \frac{\partial f_3}{\partial \sigma} : \Xi : \frac{\partial f_3}{\partial \sigma} \tag{A.16a}$$

$$a_{12} = \frac{\partial f_3}{\partial \sigma} : \Xi : \frac{\partial^2 f_3}{\partial \sigma \partial k} - \frac{1}{\Delta\lambda_3} \frac{\partial f_3}{\partial k} \tag{A.16b}$$

$$a_{21} = \frac{\partial^2 f_3}{\partial \sigma \partial k} : \Xi : \frac{\partial f_3}{\partial \sigma} + \frac{1}{\Delta\lambda_3} \frac{\partial f_3}{\partial J} \tag{A.16c}$$

$$a_{22} = \frac{\partial^2 f_3}{\partial \sigma \partial k} : \Xi : \frac{\partial^2 f_3}{\partial \sigma \partial k} + \frac{1}{\Delta\lambda_3} \frac{\partial^2 f_3}{\partial J \partial k} - \frac{1}{3\Delta\lambda_3^2} \frac{\partial(\Delta I^{\mathrm{p}}(k))}{\partial k} \tag{A.16d}$$

References

Bockstiegel, G., 1968. Relations between pore structures and densification mechanisms in the compacting of iron powder. Perspectives in Powder Metallurgy 3, 54–71.

Chorin, A., Hughes, T.J.R., McCracken, M.F., Marsden, J.E., 1978. Product formulas and numerical algorithms. Communications on Pure and Applied Mathematics 31, 205–256.

Chtourou, H., Gakwaya, A., Guillot, M., Hrairi, M., 1995a. Implementing a cap material model for the simulation of metal powder compaction. Net Shape Processing of Powder Materials, AMD-vol. 216, ASME, San Fransisco, CA, pp. 19–27.

Chtourou, H., Guillot, M., Gakwaya, A., 1995b. Modeling the rigid die compaction of 316L stainless steel powder. Advances in Powder Metallurgy and Particular Materials, Seattle, vol. 1 (part 2), pp. 169–183.

Chtourou, H., Gakwaya, A., Guillot, M., Hrairi, M., 1996. Finite element simulation of the rigid die compaction of metal powder components. Proceedings of the Canadian Society of Mechanical Engineers Forum. McMaster University.

Chtourou, H., Guillot, M., Gakwaya, A., 2001. Modeling of the metal powder compaction process using the cap model. Part I. Experimental material characterization and validation. International Journal of Solids and Structures 39 (4), 1059–1075.

Crawford, J., Lindskog, P., 1983. Constitutive equations and their role in the modeling of the cold pressing process. Scandinavian Journal of Metallurgy 12, 271–281.

Dhatt, G.S., Touzot, G., 1984. In: Maloine, S.A. (Ed.), Une présentation de la Méthode des éléments finis.

Dimaggio, F., Sandler, I., 1971. Material models for granular soils. Journal of the Engineering Mechanics Division, ASCE, vol. 97, pp. 935–950.

German, R.M., 1984. Powder Metallurgy Science. MPIF, Princeton, NJ.

Guillot, M., Chtourou, H., 1996. Generalization of the Vickers hardness local density measurement technique to different powder materials. In: Proceedings of the World Congress on Powder Metallurgy and Particulate Materials, Washington, DC, vol. 1 (part 4), pp. 31–40.

Gurson, A.L., Posteraro, R.A., 1992. Yield functions for metal powders for use in the numerical simulation of powder compaction. TMS Conference, San Diego, CA.

HKS Inc., 1995a. ABAQUS-Post User Guide, Version 5.4. Hibbit, Karlsson and Sorensen, Inc., Rhode Island.

HKS Inc., 1995b. ABAQUS Theory Manual, Version 5.4. Hibbit, Karlsson and Sorensen, Inc., Rhode Island.

Hofstetter, G., Simo, J.C., Taylor, R.L., 1993. A modified cap model: closest point solution algorithms. Computers and Structures 46 (2), 203–214.

Koopman, M.G., Rachakonda, V.B.S., Gurson, A.L., McCabe, T., 1992. Material models for the finite element simulation of compaction of metal powder. TMS Fall Meeting, Chicago.

Kröner, E., 1960. Archive for Rational Mechanics and Analysis 4, 273.

Lee, E.H., Liu, D.T., 1967. Finite strain elastic–plastic theory with application to plane waves analysis. Journal of Applied Physics 38, 19–27.

Lenel, F.V., 1980. Powder Metallurgy, Principles And Applications. MPIF, Princeton, NJ.

Mandel, J., 1971. Plasticité classique et viscoplasticité CISM no. 97 Udine, Springer, Vienna.

Peric, D., Owen, D.R.J., Honnor, M.E., 1992. A model for finite strain elasto-plasticity based on logarithmic strains: computational issues. Computer Methods in Applied Mechanics and Engineering 94, 35–61.

Sandler, I.S., Rubin, D., 1979. An algorithm and a modular subroutine for the cap model. International Journal for Numerical and Analytical Methods in Geomechanics 3, 173–186.

SDRC Corporation, 1994. Ideas Master Series Student Guide.

Shima, S., Saleh, M.A.E., 1993. Variation of density distribution in compacts in closed die compaction with powder characteristics. Advances in Powder Metallurgy and Particulate Materials 3, 175–189.

Simo, J.C., 1992. Algorithms for static and dynamic multiplicative plasticity that preserve the classical return maping schemes of the infinitesimal theory. Computer Methods in Applied Mechanics and Engineering 99, 62–112.

Simo, J.C., Ortiz, M., 1985. A unified approach to finite deformation elastoplasticity based on the use of hyperelastic constitutive equations. Computer Methods in Applied Mechanics and Engineering 49, 222–245.

Simo, J.C., Ju, J.W., Pister, K.S., Taylor, R.L., 1988a. Assessment of cap model: consistent return algorithms and rate dependent extension. ASCE Journal of Engineering Materials 114 (2), 191–218.

Simo, J.C., Kennedy, J.G., Govindje, S., 1988b. Non-smooth multisurface plasticity and viscoplasticity. Loading/unloading conditions and numerical algorithms. International Journal for Numerical Methods in Engineering 26, 2161–2185.

Trasorras, J., Krauss, T.M., Fergusson, B.L., 1989. Modeling the powder compaction using the finite element method. In: Proceedings of the 1989 International Conference on Powder Metallurgy, San Diego, CA, pp. 85–104.

Weber, G.G., Brown, S.B., 1989. Simulation of the compaction of powder components. Advances in Powder Metallurgy and Particulate Materials 1, 105–118.